Supplementary information

Continuous filtration of multi-metal contaminated river and groundwater using antioxidant preserved redox-sensitive nanocomposites: ultrahigh reactivity and self-sedimentation possibility

Nitin Khandelwal[a], Jai Kishan Rajak[a], Nisha Singh[a], Ekta Tiwari[a], Zahid Ahmad Ganie[a], Aniket Choudhary[a], Gopala Krishna Darbha[a,b,*]

[a] Environmental Nanoscience Laboratory, Department of Earth Sciences, Indian Institute of Science Education and Research Kolkata, Mohanpur, West Bengal, India- 741246

[b] Centre for Climate and Environmental Studies, Indian Institute of Science Education and Research Kolkata, Mohanpur, West Bengal, India, 741246

[*]Corresponding author: Gopala Krishna Darbha, Email- gkdarbha@gmail.com, gkdarbha80@yahoo.com Tel: (+91)- 9849626082

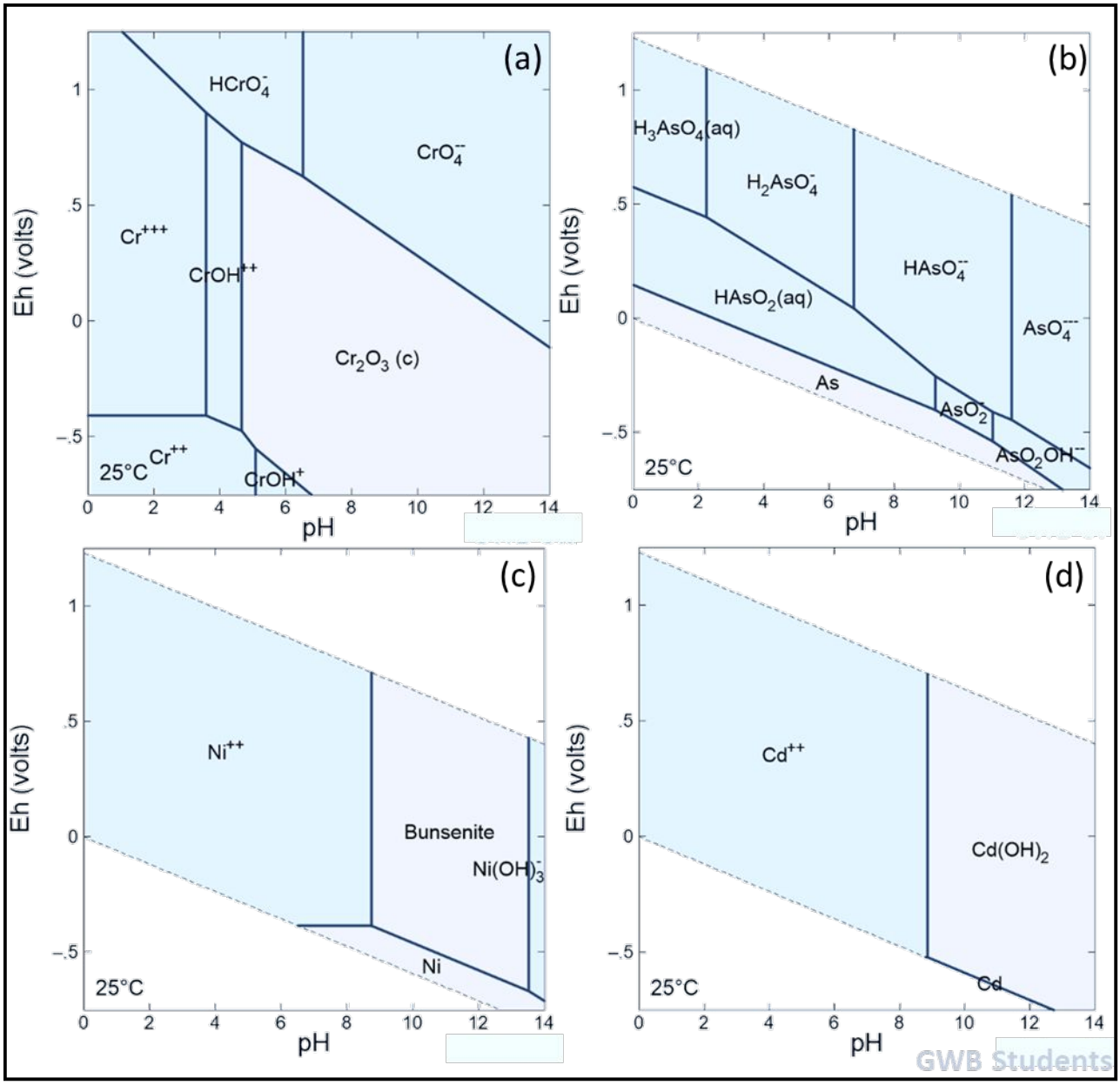

Fig. S1 Eh-pH speciation diagrams for (a) CrO_4^{2-}, (b) AsO_2^-, (c) Ni^{2+} and (d) Cd^{2+}

Section-1

1.1 Materials and methods: characterization

Synthesized composites and raw materials were characterized for morphology and composition using scanning and transmission electron microscopy (Carl Zeiss SUPRA 55VP FESEM and UHR-FEG-TEM, JEOL, JEM 2100 F model using a 200 kV electron source, respectively) both associated with EDAX (Oxford INCA).

For obtaining crystallinity, powder x-ray diffraction data was obtained using Rigaku (mini flex, Japan) benchtop powder X-ray diffractometer having Cu Kα = 1.54059 Å radiation at 40 kV/15 mA. Scanning range and scanning rates were 5^{o} to 65^{o} 2θ and 5° 2θ per minute respectively.

Point of zero charge (pH_{PZC}) and zeta potential of suspension was measured through a dynamic light scattering (DLS) instrument using Zetasizer, Malvern, UK. Surface functionality of the materials was analyzed using Fourier transformation infrared spectroscopy (FTIR, Nicolet I5, Thermoscientific) using KBr pallet method. Almond skin extracts (Antioxidants) concentrations were qualitatively observed using UV-Vis spectrophotometer (Evolution 201, Thermoscientifc) before and after the modification of composites. Surface redox state and composition of elements was studied with the help of X-ray Photoelectron Spectroscopy (XPS, Nexsa, Thermofisher-Scientific) incorporating Al Kα as the source of X-ray.

1.2 Synthesis of antioxidant capped biochar-iron (ASBC-I) nanocomposites

As shown in fig. 1, for stage-1 modification, biochar powders were dispersed in antioxidants solution and sonicated. Then, antioxidant modified biochar was dispersed in 4:1 ethanol: water interfacial iron solution (Fe/BC mass ratio= 1). The suspension was sonicated (30 min) and shaken (30 min) sequentially to allow iron to homogeneously interact with the biochar surface. Later, $NaBH_4$ solution (0.94 M) was added dropwise under continuous stirring for the reduction

and formation of elemental iron nanoparticles on biochar surface [1, 2]. After complete addition, the reaction mixture was vigorously stirred for another 20 minutes to assure complete reduction. Then the precipitate was filtered and washed with ethanol. In the stage-2 modification, washed precipitates were added to the antioxidant solution and sonicated to assure proper antioxidant capping of the composite. The obtained composites after stage-2 modification are denoted as ASBC-I nanocomposites i.e., ASBC-I-550 and ASBC-I-750, respectively denoting the pyrolysis temperature of biochar surface used. In the end, composites were separated from the antioxidant solution, washed with ethanol, vacuum dried, and stored for further use. Schematic representation of the synthesis scheme is provided in fig. 1.

Table-S1 Physiochemical parameters of utilized water samples

S. No.	Component	Concentration		
		Groundwater	**River water**	**Synthetic Rain water**
1	SO_4^{2-} (mM)	0.14	0.22	0.028
2	Cl^- (mM)	0.93	0.69	0.007
3	HCO_3^- (mM)	4.5	1.22	-
4	NO_3^- (mM)	0.05	0.038	0.008
5	Na^+ (mM)	1.3	0.57	0.008
6	Ca^{2+} (mM)	2.8	0.46	0.0002
7	Mg^{2+} (mM)	0.95	0.22	0.001
8	K^+ (mM)	0.02	0.063	0.0012
9	Humic Acid (mg/L)	3.5	1.85	-
10	pH	7.4	7.6	4.3
11	Ionic strength	11 X 10^{-3} M	2.3×10^{-3} M	0.31 X 10^{-3} M

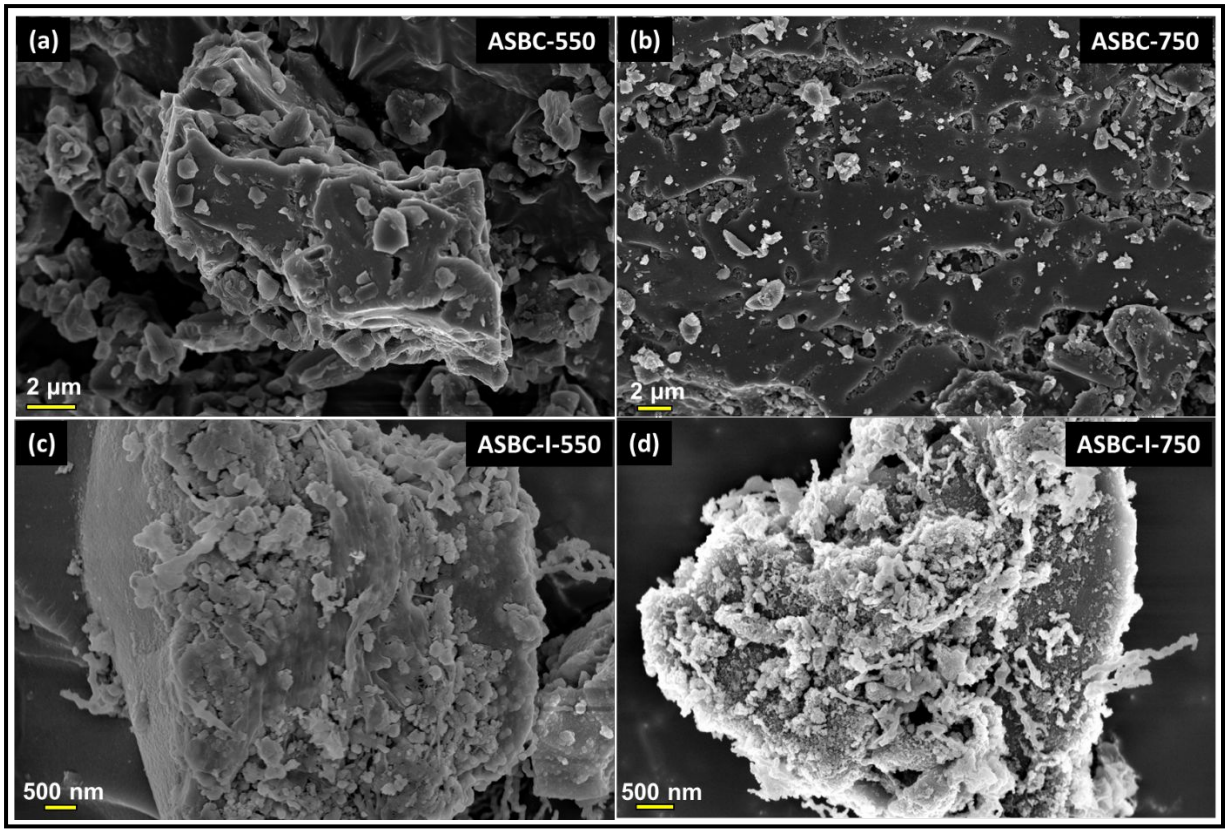

Fig. S2 FESEM images of (a) ASBC-550, (b) ASBC-750, (c) ASBC-I-550 and (d) ASBC-I-750 composites.

Table-S2 Elemental composition of raw biochar and synthesized composite (in atomic%)

	C	**N**	**O**	**Fe**
ASBC-550	42.7	46.8	10.5	-
ASBC-750	44.6	49.2	6.2	-
ASBC-I-550	20.1	17.9	33.1	28.7
ASBC-I-750	23.7	23.1	25.2	27.9

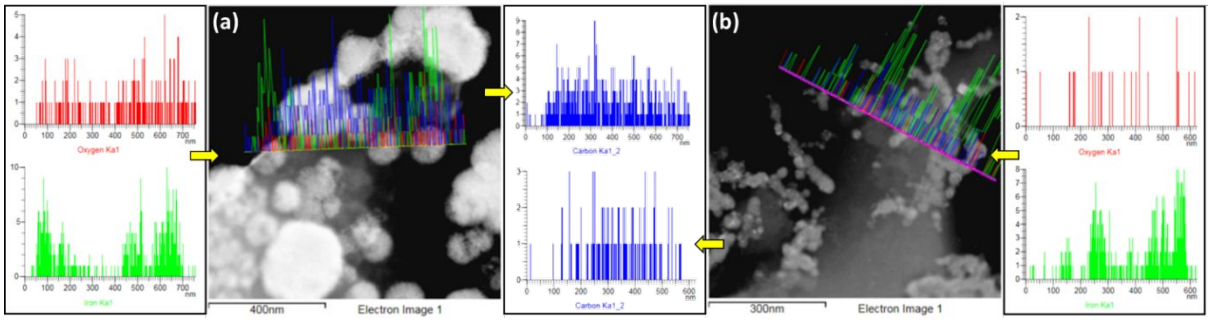

Fig. S3 TEM elemental line scans along nZVI particles in (a) ASBC-I-550 and (b) ASBC-I-750 composites

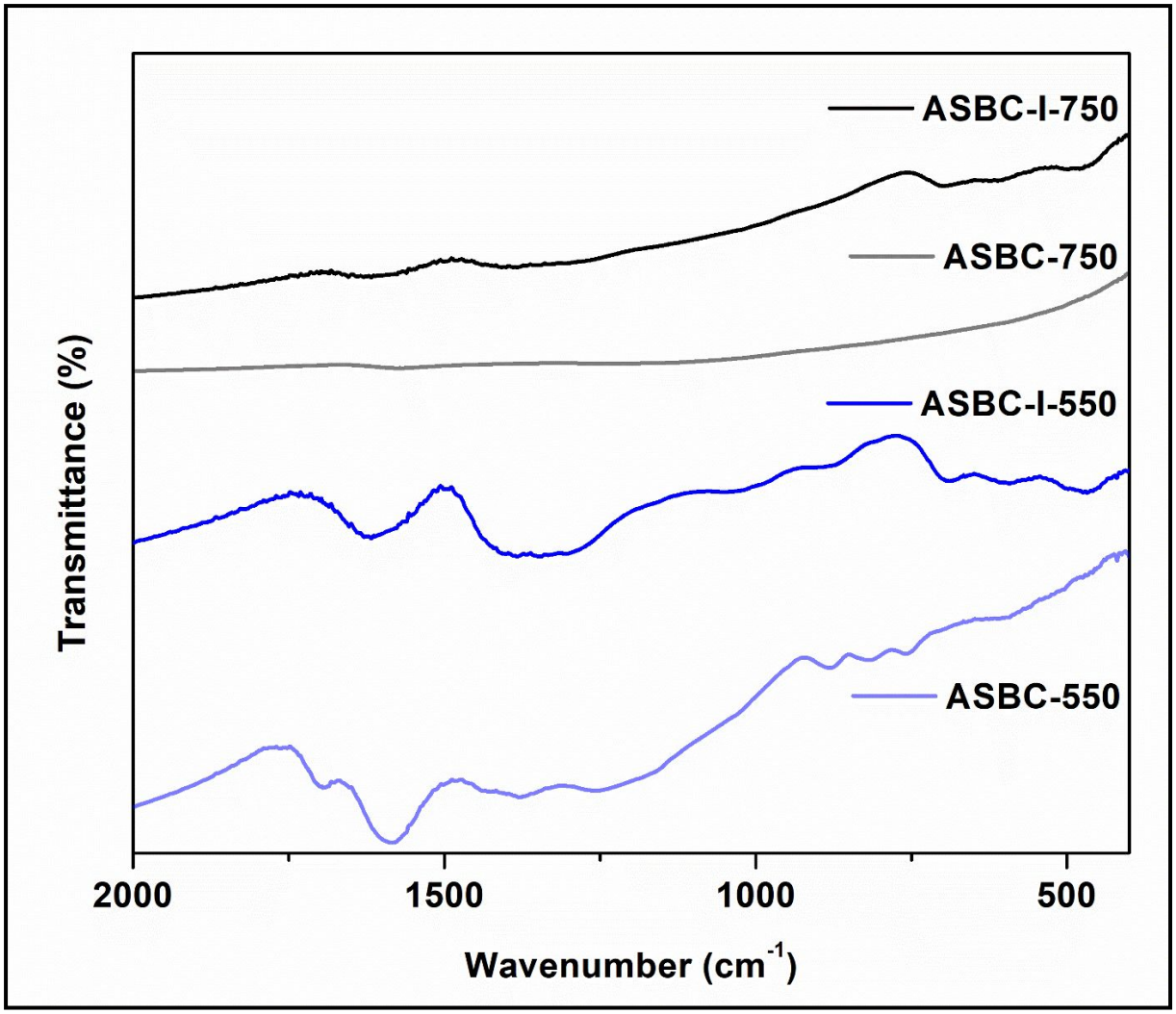

Fig. S4 FTIR spectra of biochar and nanocomposites

1.4 FTIR Analysis: surface functionality of the composites

FTIR spectra in fig. S4 shows that peaks associated with ASBC-550 such as- 1694 cm^{-1} (C=O/ N-H stretching), 1585 cm^{-1} (C=C cyclic alkene stretching), 1437 cm^{-1} (C-H_2 stretching and O-H bending due to alcohol), 1378 cm^{-1} (O=C-O stretching), and 873 cm^{-1} (aromatic C-H out-of-plane deformation) were decreased and disappeared at higher pyrolysis temperature biochar i.e. ASBC-750 [3]. After the growth of iron nanoparticles on the surface, these peaks of ASBC-550 in the region 1400-1700 cm^{-1} disappeared whereas a sharp decrease was observed in the intensity of peaks in the region 700-900 cm^{-1} with a slight shift. Simultaneously, various new peaks corresponding to iron nanoparticles appeared, suggesting that ASBC-I composites are

not just a physical mixture of particles and surface and include various chemical interactions. Major FTIR peaks in ASBC-I-550 and ASBC-I-750 were 1630 cm^{-1} (O-H stretching of H_2O and FeOOH), 690 cm^{-1} (symmetric Fe-O stretching), 590 cm^{-1} (Fe-O stretching modes of tetrahedral and octahedral sites), and 470 cm^{-1} (Fe-O stretching due to Hematite)[4].

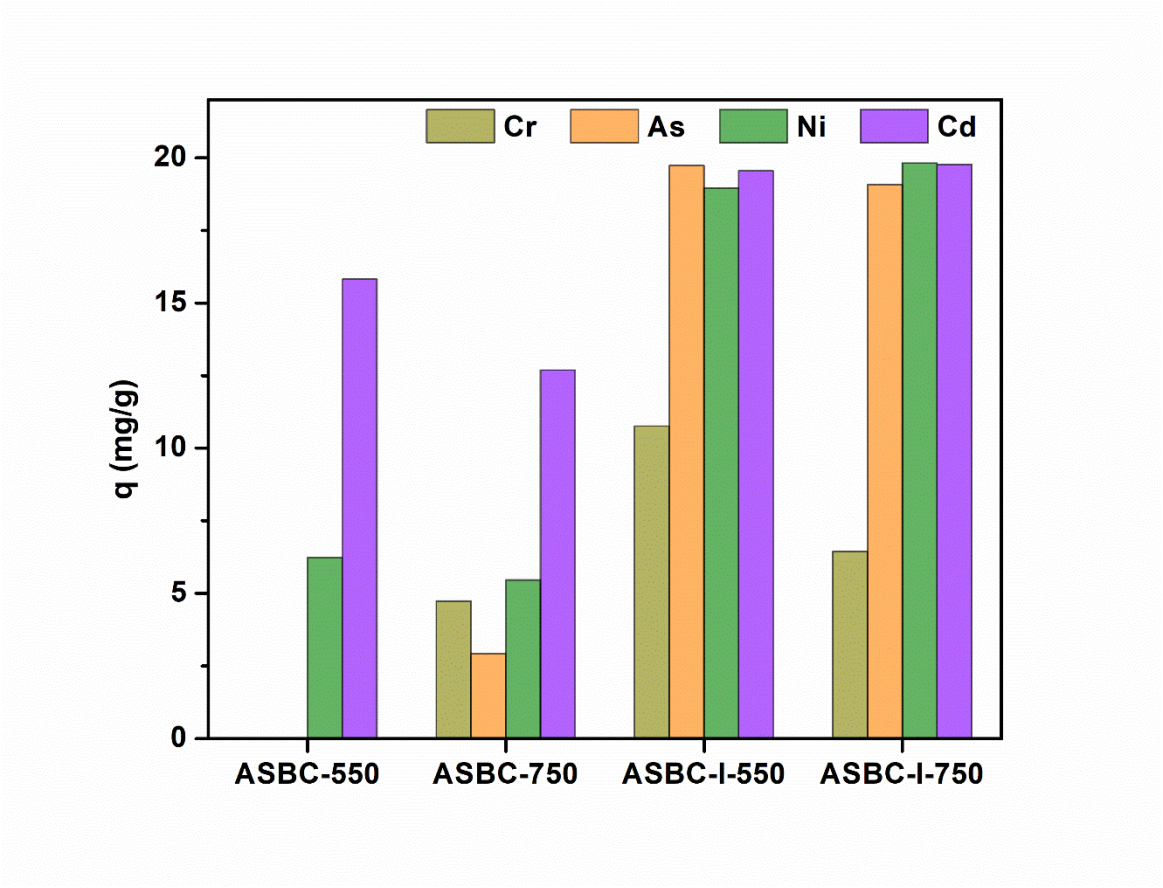

Fig. S5 Sorption capacities of biochar and respective nanocomposites for different metallic species

Section-2

Non-linear kinetics modelling

Kinetic models	Non-linear equations
pseudo-first-order	$q_t = q_e.\,[1 - \exp(-k_1.t)]$
pseudo-second-order	$q_t = q_e - \dfrac{q_e}{[k_2\,(q_e).t + 1]}$
General order	$q_t = q_e - \dfrac{q_e}{[k_N\,(q_e)^{n-1}.t.\,(n-1)+1]^{\frac{1}{1-n}}}$
Intra-particle diffusion (IPD)	$q_t = k_i\sqrt{t} + C$

Where:

q_e = Equilibrium sorption capacity (mg/g) , q_t = Sorption capacity at time= t (mg/g)

k_1 = pseudo-first-order reaction rate constant (min^{-1}) , k_2 = second order reaction rate constant (g $mg^{-1}min^{-1}$), k_N = General order reaction rate constant [min^{-1} (g $mg^{-1})^{n-1}$] and k_i = intra particle diffusion rate constant (mg/g $hr^{0.5}$)

n= order of the reaction and intercept C gives resistance in mass transfer due to boundary layer

Both the kinetic models i.e. pseudo 1st and 2nd order are with presumed orders for the uptake of the contaminants. For example- pseudo 2nd order assumes that the rate of uptake of adsorbate is of 2nd order with respect to all the available sorption sites[5]. Logically, it would be better to obtain the order of a reaction kinetics from the experimental data itself rather than assuming any order. As the process of adsorption is considered to be the rate determining step, it helped in establishing the general order kinetic model. Which states that "the order of sorption process should follow the same trend as that of a chemical reaction, where the order of the reaction is

not being restrained by a given model but experimentally" [6, 7]. Whereas, intra particle diffusion (IPD) is based on Fick's second law of diffusion [8].

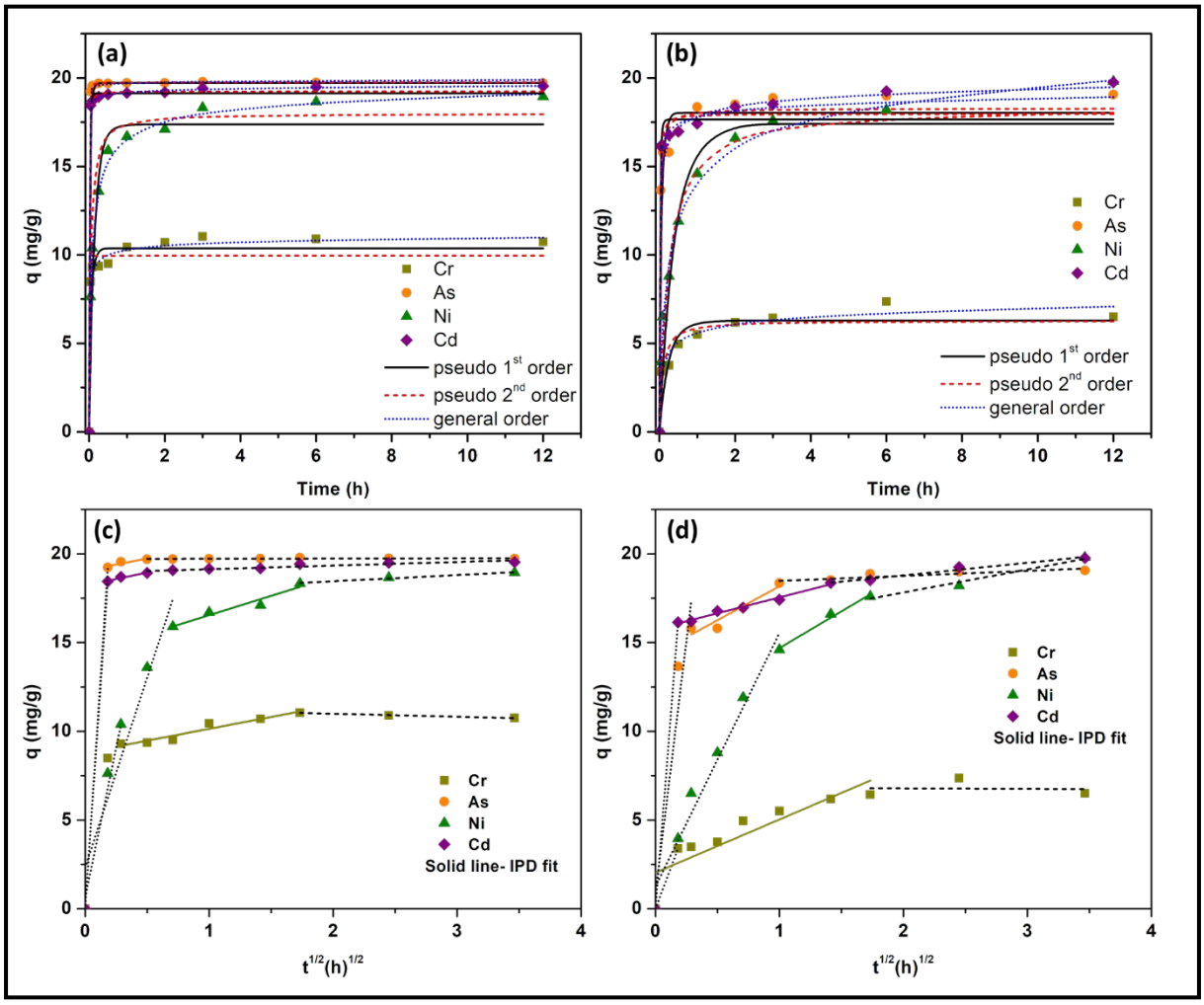

Fig. S6 experimental kinetic data and various fitted kinetic models i.e. pseudo first order, pseudo second order and general order for (a) ASBC-I-550 and (b) ASBC-I-750, and (c, d) IPD modelling for ASBC-I-550 and ASBC-I-750 respectively

Table S3 parameters obtained for fitted kinetic models and calculated errors

Kinetic models		Pseudo first order			Pseudo second order			General order				Intraparticle diffusion (IPD)		
Adsorbate		K_1 (h^{-1})	q (mg/g)	R^2	K_2 (g $mg^{-1}h^{-1}$)	q (mg/g)	R^2	K_n (h^{-1})	q (mg/g)	n	R^2	K (mg/g $h^{1/2}$)	Intercept	R^2
CrO_4^{2-}	ASBC-I-550	26.94	10.37	0.93	2859.29	9.95	0.93	5.38E-02	11.77	5.03	0.99	1.33	8.80	0.92
	ASBC-I-750	4.60	6.29	0.83	2.49	6.28	0.88	9.40E-06	10.16	7.44	0.95	2.99	2.04	0.74
AsO_2^-	ASBC-I-550	56.96	19.73	0.98	113.40	19.75	1.00	6.44E-02	20.72	13.39	1.00	1.34	19.07	0.68
	ASBC-I-750	24.53	18.03	0.94	4.27	18.28	0.98	3.82E-04	21.75	5.68	1.00	3.83	14.34	0.87
Ni^{2+}	ASBC-I-550	8.65	17.38	0.90	1.74	18.00	0.93	1.55E-02	20.48	3.44	0.99	2.18	14.37	0.91
	ASBC-I-750	2.67	17.42	0.94	0.25	18.36	0.97	5.42E-06	26.94	5.20	0.99	4.13	10.55	0.97
Cd^{2+}	ASBC-I-550	99.10	19.14	1.00	31.54	19.24	1.00	1.94E-02	20.48	8.53	1.00	1.45	18.22	0.91
	ASBC-I-750	71.75	17.66	0.96	10.90	17.97	0.97	8.03E-07	22.06	9.25	0.99	1.79	15.76	0.98

Kinetic models		Pseudo first order					Pseudo second order					General order				
Adsorbate		SSE	RMSE	ARE	Chi-square	HYBRID	SSE	RMSE	ARE	Chi-square	HYBRID	SSE	RMSE	ARE	Chi-square	HYBRID
CrO_4^{2-}	ASBC-I-550	6.247	0.901	2.334	1.149	11.405	7.208	0.772	-0.485	0.599	7.709	2.212	0.258	0.163	0.067	0.969
	ASBC-I-750	7.477	1.046	9.039	8.557	36.331	5.345	0.709	0.394	1.351	14.528	3.321	0.406	0.222	0.412	5.658
AsO_2^-	ASBC-I-550	2.611	0.779	1.281	0.362	3.946	0.513	0.088	-0.218	0.004	0.050	0.708	0.073	-0.001	0.003	0.039
	ASBC-I-750	10.603	1.440	2.086	1.715	17.698	5.811	0.684	-0.108	0.269	3.533	3.089	0.365	-0.042	0.081	1.166
Ni^{2+}	ASBC-I-550	12.531	1.439	4.247	3.183	26.452	11.188	1.329	-7.055	1.302	19.427	2.186	0.270	0.009	0.050	0.717
	ASBC-I-750	12.457	1.415	9.455	7.052	41.020	8.102	0.827	4.366	1.551	13.969	3.987	0.481	1.179	0.276	3.913
Cd^{2+}	ASBC-I-550	1.825	0.213	-0.012	0.024	0.298	1.416	0.141	-0.005	0.010	0.130	0.296	0.044	-0.001	0.001	0.014
	ASBC-I-750	8.608	0.845	-0.222	0.405	5.045	7.543	0.683	-0.138	0.266	3.294	3.605	0.340	0.058	0.066	0.941

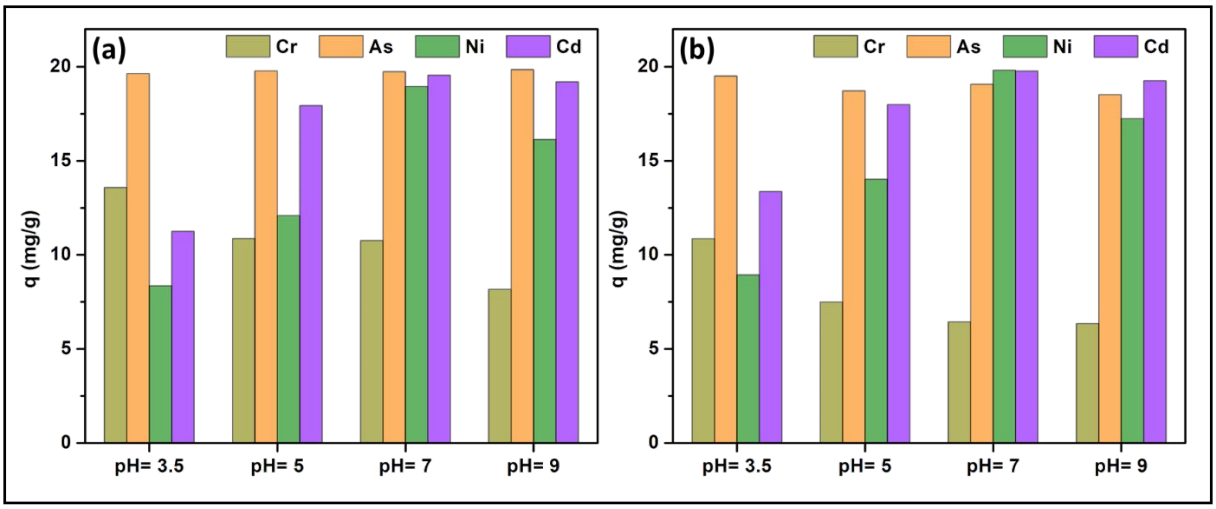

Fig. S7 Effect of solution pH on the sorption capacities of (a) ASBC-I-550 and (b) ASBC-I-750 nanocomposites for various metals

Section-3: Adsorption Isotherm models

Isotherm models	Non-linear equations
Langmuir	$q_e = \frac{q_m K_L C_e}{1 + K_L C_e}$
Freundlich	$q_e = K_F C_e^n$
Sip	$q = q_{max} \frac{K[C_e]^n}{1 + K[C_e]^n}$

Where:

C_e (mg/L) = equilibrium concentration,

q_e = sorption capacity at equilibrium (mg/g),

q_m = obtained maximum sorption capacity (mg/g) and

K_L = Langmuir constants (L/mg) related to energy of adsorption

K_F = Freundlich adsorption constant (mg/g)(L/mg)$^{1/n}$ and

n = a measure of the adsorption intensity (Freundlich)

K = Sips isotherm constant

n = Sips isotherm exponent

Isotherm is generally utilized to evaluate interactions between adsorbate and adsorbent. Commonly used isotherms include Langmuir model which assumes monolayer sorption of the adsorbate on adsorbent surface. It suggests that all the sorption sites are identical and energetically equivalent [9, 10]. Freundlich model assumes heterogeneous nature of the surface and represents initial sorption on surface followed by condensation effect causing strong adsorbate-adsorbent interaction. To depict isotherm data better, Sip's isotherm model can be used. This model is a combination of both Langmuir and Freundlich model. At low adsorbate concentration this model predicts Freundlich like behavior which converts to plateau or monolayer sorption at higher concentrations [11].

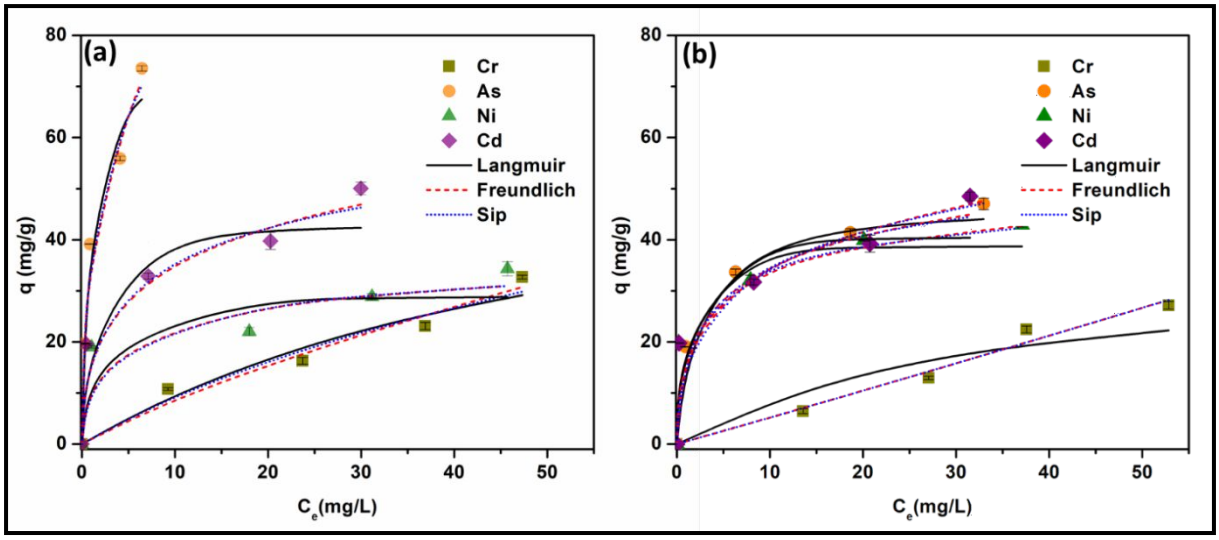

Fig. S8 Effect of contaminant concentration and various fitted sorption isotherm models for (a) ASBC-I-550 and (b) ASBC-I-750 nanocomposites in monometallic system

Table S4 parameters obtained for fitted isotherm models in monometallic system and calculated errors

Sorption isotherm models	Mono-metallic system	Langmuir			Freundlich			Sips			
Adsorbate		q_{max} (mg/g)	K_L	R^2	K_f	n	R^2	q_{max} (mg/g)	K	n	R^2
CrO_4^{2-}	ASBC-I-550	59.94	0.02	0.95	1.45	0.79	0.97	118.72	0.01	0.85	0.97
	ASBC-I-750	34.65	0.03	0.95	0.49	1.02	0.96	68.59	0.01	1.02	0.96
AsO_2^-	ASBC-I-550	76.59	1.15	0.97	36.09	0.36	0.98	167.95	0.28	0.50	0.98
	ASBC-I-750	46.16	0.63	0.95	20.58	0.24	0.99	97.30	0.26	0.32	0.99
Ni^{2+}	ASBC-I-550	29.16	1.62	0.90	16.92	0.16	0.95	100.30	0.20	0.22	0.94
	ASBC-I-750	38.91	5.18	0.83	24.65	0.15	0.99	130.21	0.24	0.21	0.98
Cd^{2+}	ASBC-I-550	43.28	1.50	0.93	21.65	0.23	0.98	134.06	0.19	0.29	0.98
	ASBC-I-750	40.73	3.72	0.71	23.27	0.19	0.93	100.96	0.29	0.29	0.91

Isotherm models	Mono-metallic system	Langmuir					Freundlich					Sips				
Adsorbate		SSE	RMSE	ARE	Chi-square	HYBRID	SSE	RMSE	ARE	Chi-square	HYBRID	SSE	RMSE	ARE	Chi-square	HYBRID
CrO_4^{2-}	ASBC-I-550	10.262	2.406	-0.914	1.318	45.024	7.884	1.782	1.816	1.057	31.433	9.040	2.059	-0.042	1.050	52.224
	ASBC-I-750	16.063	3.652	-13.229	4.197	181.405	5.411	1.379	-2.181	0.524	16.750	5.411	1.379	-2.181	0.524	25.125
AsO_2^-	ASBC-I-550	15.375	4.288	0.811	1.500	51.874	14.253	3.309	-1.386	1.381	45.927	14.435	3.391	-1.110	1.211	61.356
	ASBC-I-750	9.320	2.206	0.914	0.739	24.266	3.527	0.955	-0.533	0.166	5.520	2.533	0.731	-0.211	0.096	4.767
Ni^{2+}	ASBC-I-550	12.444	3.714	-1.705	2.430	88.068	10.232	2.715	-0.575	1.397	50.642	10.891	2.828	-0.276	1.559	83.744
	ASBC-I-750	11.863	3.298	-0.607	1.427	51.558	3.440	0.911	0.161	0.128	4.386	4.683	1.190	0.318	0.226	11.665
Cd^{2+}	ASBC-I-550	18.355	4.736	-0.295	2.827	94.517	8.646	2.131	0.410	0.573	19.105	10.027	2.399	0.395	0.734	36.295
	ASBC-I-750	18.355	4.736	-0.295	2.827	94.517	8.646	2.131	0.410	0.573	19.105	10.027	2.399	0.395	0.734	36.295

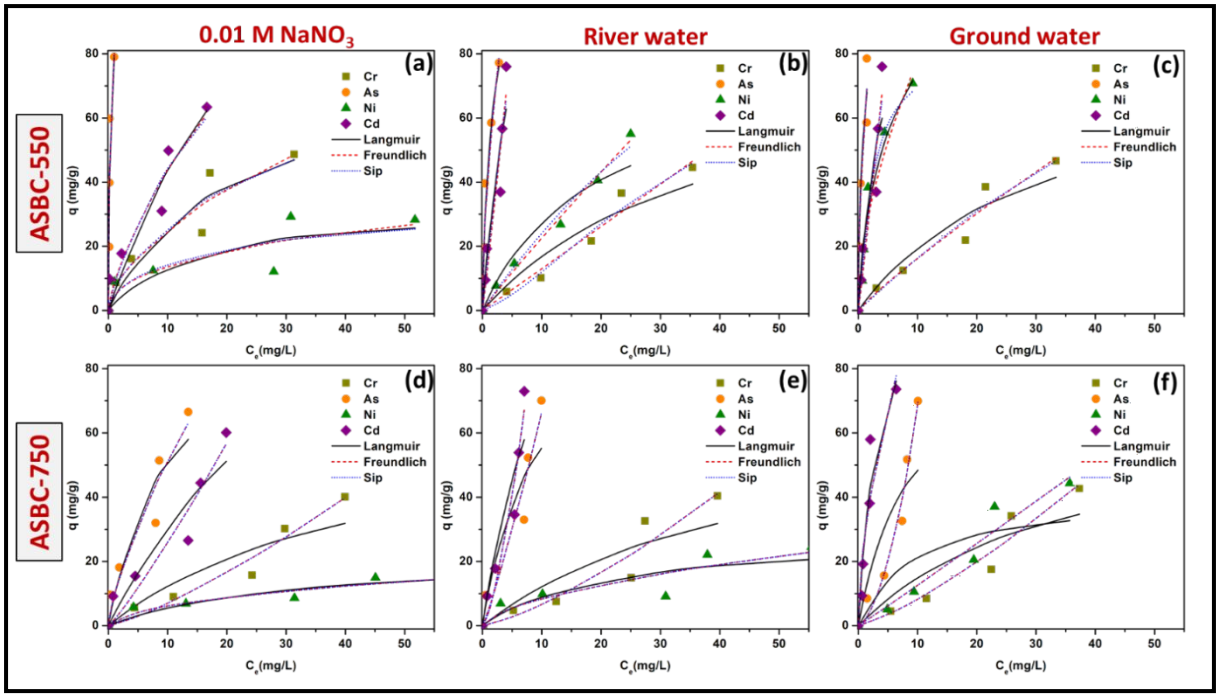

Fig. S9 Effect of contaminant concentration and various fitted sorption isotherm models for (a-c) ASBC-I-550 and (d-f) ASBC-I-750 nanocomposites in 0.01M $NaNO_3$, river water and groundwater solutions respectively, in multi-metallic system

Table S5 parameters obtained for fitted isotherm models for CrO_4^{2-} removal in multi-metallic system and calculated errors

Sorption isotherm models	CrO_4^{2-}	Langmuir			Freundlich			Sips			
Waters		q_{max} (mg/g)	K_L	R^2	K_f	n	R^2	q_{max} (mg/g)	K	n	R^2
0.01 M $NaNO_3$	ASBC-I-550	72.81	0.06	0.91	7.17	0.56	0.92	125.97	0.06	0.69	0.92
	ASBC-I-750	64.05	0.02	0.88	0.35	1.29	0.96	107.86	0.00	1.29	0.96
River water	ASBC-I-550	79.65	0.03	0.93	1.27	1.01	0.97	94.71	0.00	1.49	0.97
	ASBC-I-750	66.31	0.02	0.82	0.28	1.36	0.91	85.35	0.00	1.36	0.91
Groundwater	ASBC-I-550	76.40	0.04	0.93	2.15	0.88	0.95	157.70	0.01	1.05	0.95
	ASBC-I-750	64.74	0.03	0.85	0.41	1.29	0.95	107.86	0.00	1.29	0.95

Isotherm models	CrO_4^{2-}	Langmuir					Freundlich					Sips				
Adsorbate		SSE	RMSE	ARE	Chi-square	HYBRID	SSE	RMSE	ARE	Chi-square	HYBRID	SSE	RMSE	ARE	Chi-square	HYBRID
0.01M $NaNO_3$	ASBC-I-550	25.135	5.459	5.414	7.519	191.550	18.426	4.962	-1.477	4.399	124.195	20.071	5.094	-1.513	4.548	183.779
	ASBC-I-750	24.921	5.286	-14.468	6.987	221.404	13.087	2.837	8.588	6.378	102.956	13.086	2.837	8.584	6.375	137.261
River water	ASBC-I-550	24.750	4.723	-17.519	5.990	205.044	13.402	2.915	-2.649	2.043	50.867	12.960	2.596	3.463	2.923	75.340
	ASBC-I-750	34.636	6.702	-28.504	12.235	442.852	18.637	4.395	0.989	6.523	158.022	18.637	4.395	0.989	6.523	210.696
Groundwater	ASBC-I-550	22.963	4.744	-8.432	4.610	137.064	14.581	3.554	0.261	2.713	69.856	14.267	3.601	1.200	3.074	108.173
	ASBC-I-750	35.866	6.727	-37.904	12.775	524.925	15.306	3.598	-1.458	3.253	81.862	15.307	3.598	-1.459	3.253	109.152

Table S6 parameters obtained for fitted isotherm models for AsO_2^- removal in multi-metallic system and calculated errors

Sorption isotherm models	AsO_2^-	Langmuir			Freundlich			Sips			
Waters		q_{max} (mg/g)	K_L	R^2	K_f	n	R^2	q_{max} (mg/g)	K	n	R^2
0.01 M $NaNO_3$	ASBC-I-550	100.70	3.85	0.85	81.03	0.42	0.85	300.28	0.37	0.50	0.85
	ASBC-I-750	94.52	0.12	0.90	10.36	0.69	0.94	97.74	0.12	0.71	0.94
River water	ASBC-I-550	106.41	0.90	0.95	45.18	0.54	0.94	299.93	0.18	0.65	0.94
	ASBC-I-750	96.42	0.13	0.87	4.52	1.17	0.94	97.79	0.05	1.17	0.94
Groundwater	ASBC-I-550	84.44	2.82	0.95	58.40	0.45	0.96	300.25	0.25	0.52	0.96
	ASBC-I-750	82.14	0.14	0.78	0.90	1.8	0.97	97.77	0.01	1.88	0.97

Isotherm models	AsO_2^-	Langmuir					Freundlich					Sips				
Adsorbate		SSE	RMSE	ARE	Chi-square	HYBRID	SSE	RMSE	ARE	Chi-square	HYBRID	SSE	RMSE	ARE	Chi-square	HYBRID
0.01M $NaNO_3$	ASBC-I-550	44.179	10.691	-0.399	26.144	631.816	40.800	10.828	-13.087	18.353	561.707	39.220	10.728	-10.961	17.648	740.783
	ASBC-I-750	33.827	7.278	8.328	17.407	286.205	27.814	5.907	7.177	9.681	198.997	27.872	5.915	7.239	9.789	266.706
River water	ASBC-I-550	27.636	6.116	-10.494	8.961	227.397	31.462	6.795	-14.134	11.382	333.933	28.976	6.567	-12.860	10.755	397.504
	ASBC-I-750	41.782	8.903	-2.222	12.085	319.269	30.462	6.163	14.029	33.851	285.089	30.464	6.163	14.032	33.874	380.193
Groundwater	ASBC-I-550	31.112	6.362	5.415	5.447	124.183	25.529	5.801	-4.093	3.639	98.919	24.300	5.750	-3.139	3.415	120.178
	ASBC-I-750	60.321	12.230	-26.144	23.453	774.089	18.212	4.064	12.184	23.590	165.991	18.210	4.064	12.182	23.585	221.314

Table S7 parameters obtained for fitted isotherm models for Ni^{2+} removal in multi-metallic system and calculated errors

Sorption isotherm models	Ni^{2+}	Langmuir			Freundlich			Sips			
Waters		q_{max} (mg/g)	K_L	R^2	K_f	n	R^2	q_{max} (mg/g)	K	n	R^2
0.01 M $NaNO_3$	ASBC-I-550	31.34	0.09	0.73	6.31	0.37	0.78	44.54	0.16	0.54	0.76
	ASBC-I-750	21.12	0.04	0.90	2.20	0.47	0.93	16.69	0.15	0.50	0.93
River water	ASBC-I-550	75.42	0.06	0.94	2.66	0.93	0.99	168.05	0.02	1.03	0.98
	ASBC-I-750	27.40	0.06	0.77	2.43	0.56	0.83	17.17	0.16	0.59	0.83
Groundwater	ASBC-I-550	98.36	0.29	0.98	22.99	0.53	0.95	72.69	0.40	1.65	0.99
	ASBC-I-750	40.35	0.12	0.75	1.19	1.03	0.95	52.10	0.02	1.03	0.95

Isotherm models	Ni^{2+}	Langmuir					Freundlich					Sips				
Adsorbate		SSE	RMSE	ARE	Chi-square	HYBRID	SSE	RMSE	ARE	Chi-square	HYBRID	SSE	RMSE	ARE	Chi-square	HYBRID
0.01M $NaNO_3$	ASBC-I-550	25.476	6.165	3.270	21.689	487.136	21.120	5.388	-5.273	7.397	323.518	23.969	5.646	-5.578	8.240	534.104
	ASBC-I-750	7.999	1.960	4.700	3.526	84.956	6.232	1.527	0.316	1.296	43.848	6.245	1.533	0.509	1.325	66.647
River water	ASBC-I-550	21.563	5.560	-10.059	4.387	150.674	9.600	1.946	5.477	1.191	34.502	12.214	2.806	2.097	1.359	68.214
	ASBC-I-750	18.636	4.533	-2.634	7.486	322.869	15.946	3.916	-2.755	5.476	253.247	16.003	3.925	-2.680	5.528	382.096
Groundwater	ASBC-I-550	15.746	4.265	-13.479	4.321	208.756	28.983	6.348	-18.069	8.029	408.837	13.997	3.131	-5.598	1.615	94.245
	ASBC-I-750	47.433	9.630	-57.550	20.062	1254.274	16.047	4.046	-7.242	3.046	95.909	16.047	4.046	-7.242	3.046	143.865

Table S8 parameters obtained for fitted isotherm models for Cd^{2+} removal in multi-metallic system and calculated errors

Sorption isotherm models	Cd^{2+}	Langmuir			Freundlich			Sips			
Waters		q_{max} (mg/g)	K_L	R^2	K_f	n	R^2	q_{max} (mg/g)	K	n	R^2
0.01 M $NaNO_3$	ASBC-I-550	171.18	0.03	0.94	9.83	0.65	0.94	224.20	0.04	0.78	0.94
	ASBC-I-750	152.30	0.03	0.90	1.75	1.16	0.94	213.56	0.01	1.16	0.94
River water	ASBC-I-550	163.40	0.16	0.90	15.37	1.07	0.93	240.08	0.08	1.10	0.91
	ASBC-I-750	157.45	0.08	0.89	3.41	1.52	0.95	191.62	0.02	1.52	0.95
Groundwater	ASBC-I-550	111.21	0.29	0.88	15.37	1.07	0.93	240.08	0.08	1.10	0.91
	ASBC-I-750	115.59	0.30	0.93	26.92	0.57	0.89	213.31	0.14	0.59	0.89

Isotherm models	Cd^{2+}	Langmuir					Freundlich					Sips				
Adsorbate		SSE	RMSE	ARE	Chi-square	HYBRID	SSE	RMSE	ARE	Chi-square	HYBRID	SSE	RMSE	ARE	Chi-square	HYBRID
0.01M $NaNO_3$	ASBC-I-550	30.120	6.712	19.890	60.174	420.921	24.956	5.917	10.025	13.207	260.430	27.391	6.316	12.082	20.248	468.718
	ASBC-I-750	28.946	7.360	7.170	17.770	372.402	27.859	6.225	18.721	50.360	403.396	27.857	6.225	18.718	50.351	605.085
River water	ASBC-I-550	34.410	9.232	-7.419	8.233	324.635	32.263	7.963	7.612	11.020	321.389	32.086	8.623	1.713	8.682	470.575
	ASBC-I-750	36.128	9.560	-10.697	9.410	355.752	30.220	6.808	18.130	27.354	373.980	30.220	6.808	18.131	27.356	560.981
Groundwater	ASBC-I-550	38.447	10.176	-14.300	10.508	410.714	32.263	7.963	7.612	11.020	321.389	32.086	8.623	1.713	8.682	470.575
	ASBC-I-750	33.233	7.907	-20.807	9.872	436.275	38.614	9.732	-24.348	14.869	668.392	38.559	9.710	-24.306	14.803	997.934

Section-4

Column transport models

Column transport models	Non-linear equations
Thomas	$\frac{C}{C_0} = \frac{1}{1 + \exp\left(\frac{k_{TH} q_0 m}{v} - k_{TH} C_0 t\right)}$
Yoon- Nelson	$\frac{C}{C_0} = \frac{\exp\left(k_{YN} t - \tau k_{YN}\right)}{1 + \exp\left(k_{YN} t - \tau k_{YN}\right)}$

Where

k_{TH}= Thomas rate constant (mL/min·mg),

q_0= adsorption capacity of the C-BC-nZVI nanotrident,

v= flow rate (mL/min),

m= adsorbent weight (g), and

t= breakthrough time (min).

k_{YN}= Yoon-nelson rate constant (mL/min·mg),

τ= time required for 50% of breakthrough (min), and

Thomas model assumes Langmuir model of adsorption-desorption kinetics in which 2nd order reversible kinetics is followed by the rate driving force and does not take axial dispersion into account[12]. Whereas, Yoon- Nelson model is simpler with the assumption that "the rate of decrease in the probability of each adsorbate molecule to be adsorbed is proportional to its adsorption probability and also to the probability of adsorbate breakthrough on the adsorbent [13]."

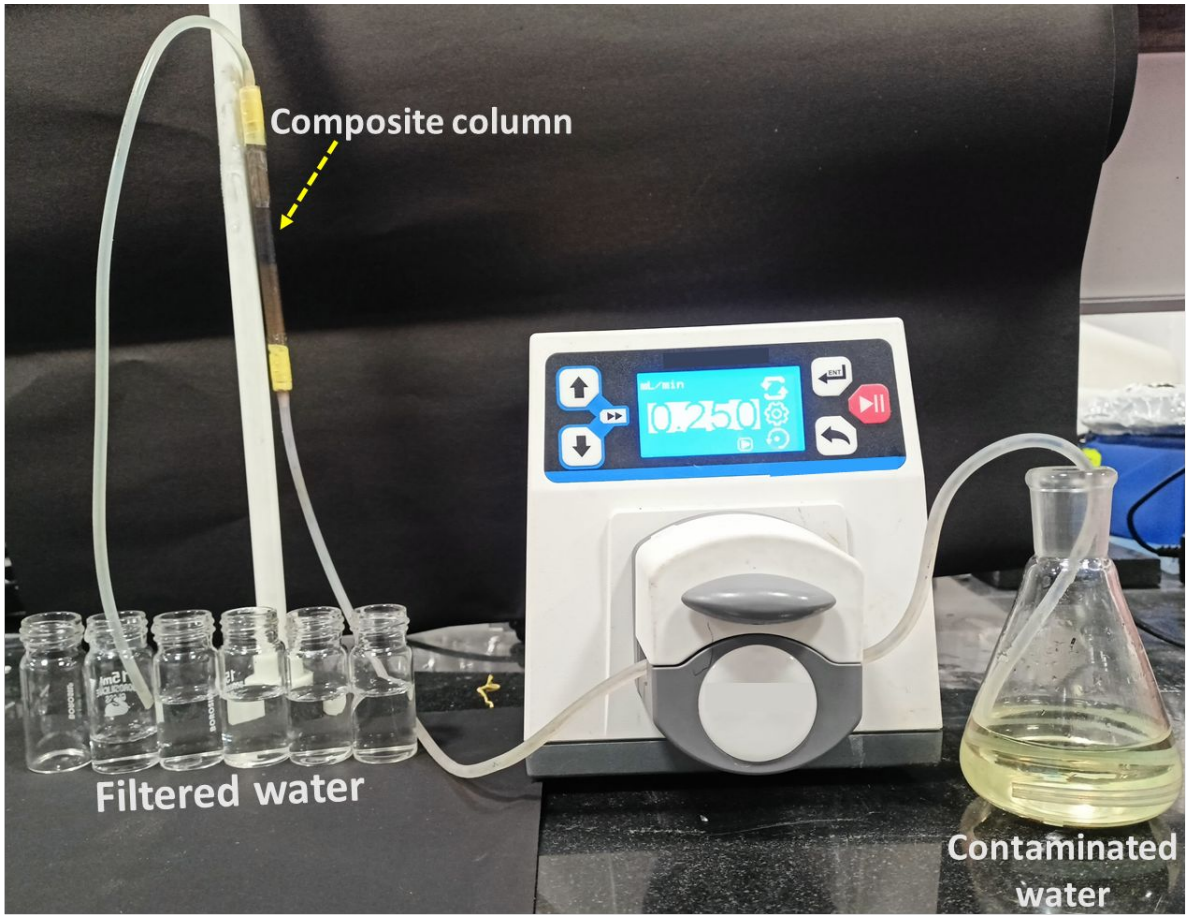

Fig. S10 Column filtration setup showing continuous removal of contaminants and generation of clean water

Table S9 parameters obtained for fitted column transport models for multi-metallic species removal in 0.01M $NaNO_3$ solutions and calculated errors

	0.01M $NaNO_3$	Thomas model							
Adsorbate		K_{TH} (L/mg.min)	q_0 (mg/g)	R^2	SSE	RMSE	ARE	Chi-square	HYBRID
CrO_4^{2-}	ASBC-I-550	1.10E-03	27.98	0.98	0.459	0.034	-5254.043	0.221	192.689
	ASBC-I-750	9.12E-04	26.30	0.95	0.638	0.041	-6245.810	0.279	243.615
AsO_2^-	ASBC-I-550	1.10E-03	27.66	0.99	0.312	0.024	-1354.465	0.159	21.011
	ASBC-I-750	9.02E-04	25.70	0.96	0.790	0.052	-4008.482	0.311	110.833
Ni^{2+}	ASBC-I-550	1.37E-03	21.55	1.00	0.319	0.023	-1120.450	0.124	11.899
	ASBC-I-750	1.08E-03	20.41	0.97	0.972	0.064	-5063.160	0.362	183.129
Cd^{2+}	ASBC-I-550	1.29E-03	25.78	0.99	0.384	0.030	-1774.440	0.134	29.354
	ASBC-I-750	9.74E-04	23.99	0.96	0.947	0.065	-3129.864	0.365	83.167
		Yoon-Nelson model							
Adsorbate		K_{YN} (h^{-1})	τ (h)	R^2	SSE	RMSE	ARE	Chi-square	HYBRID
CrO_4^{2-}	ASBC-I-550	0.66	9.33	0.98	0.459	0.034	-5254.043	0.221	192.689
	ASBC-I-750	0.55	8.77	0.95	0.638	0.041	-6245.810	0.279	243.615
AsO_2^-	ASBC-I-550	0.66	9.22	0.99	0.312	0.024	-1354.465	0.159	21.011
	ASBC-I-750	0.54	8.57	0.96	0.790	0.052	-4008.482	0.311	110.833
Ni^{2+}	ASBC-I-550	0.82	7.18	1.00	0.319	0.023	-1120.450	0.124	11.899
	ASBC-I-750	0.65	6.80	0.97	0.972	0.064	-5063.160	0.362	183.129
Cd^{2+}	ASBC-I-550	0.78	8.59	0.99	0.384	0.030	-1774.440	0.134	29.354
	ASBC-I-750	0.58	8.00	0.96	0.947	0.065	-3129.864	0.365	83.167

Table S10 parameters obtained for fitted column transport models for multi-metallic species removal in river water solutions and calculated errors

	River water	Thomas model							
Adsorbate		K_{TH} (L/mg.min)	q_0 (mg/g)	R^2	SSE	RMSE	ARE	Chi-square	HYBRID
CrO_4^{2-}	ASBC-I-550	5.96E-04	31.99	0.92	0.851	0.050	-10924.642	0.529	598.081
	ASBC-I-750	6.95E-04	50.56	0.79	0.110	0.007	-1244.638	0.071	7.432
AsO_2^-	ASBC-I-550	6.05E-04	30.39	0.93	0.872	0.052	-7746.572	0.531	321.470
	ASBC-I-750	6.69E-04	42.33	0.84	0.251	0.016	-1158.979	0.153	10.646
Ni^{2+}	ASBC-I-550	6.24E-04	32.46	0.94	0.664	0.041	-4193.944	0.380	119.078
	ASBC-I-750	7.03E-04	43.93	0.82	0.204	0.013	-652.773	0.132	3.950
Cd^{2+}	ASBC-I-550	7.17E-04	38.31	0.97	0.309	0.020	-1339.184	0.134	15.109
	ASBC-I-750	8.21E-04	50.82	0.87	0.033	0.002	-137.137	0.018	0.266
		Yoon-Nelson model							
Adsorbate		K_{YN} (h^{-1})	τ (h)	R^2	SSE	RMSE	ARE	Chi-square	HYBRID
CrO_4^{2-}	ASBC-I-550	0.36	10.66	0.92	0.851	0.050	-10924.642	0.529	598.081
	ASBC-I-750	0.42	16.84	0.79	0.110	0.007	-1244.638	0.071	7.432
AsO_2^-	ASBC-I-550	0.36	10.13	0.93	0.872	0.052	-7746.572	0.531	321.470
	ASBC-I-750	0.40	14.10	0.84	0.251	0.016	-1158.979	0.153	10.646
Ni^{2+}	ASBC-I-550	0.37	10.82	0.94	0.664	0.041	-4193.944	0.380	119.078
	ASBC-I-750	0.42	14.63	0.82	0.204	0.013	-652.773	0.132	3.950
Cd^{2+}	ASBC-I-550	0.43	12.77	0.97	0.309	0.020	-1339.184	0.134	15.109
	ASBC-I-750	0.44	17.85	0.88	0.033	0.002	-137.137	0.018	0.266

Table S11 parameters obtained for fitted column transport models for multi-metallic species removal in groundwater water solutions and calculated errors

	Groundwater	Thomas model							
Adsorbate		K_{TH} (L/mg.min)	q_0 (mg/g)	R^2	SSE	RMSE	ARE	Chi-square	HYBRID
CrO_4^{2-}	ASBC-I-550	9.07E-04	31.38	0.95	0.509	0.039	-1878.581	0.182	25.005
	ASBC-I-750	8.14E-04	42.70	0.87	0.060	0.004	-9333.129	0.043	43.270
AsO_2^-	ASBC-I-550	6.75E-04	27.48	0.93	0.753	0.045	-5437.260	0.285	197.924
	ASBC-I-750	8.18E-04	32.41	0.89	0.392	0.023	-1305.203	0.155	12.136
Ni^{2+}	ASBC-I-550	5.66E-04	38.00	0.91	0.564	0.042	-2892.621	0.225	55.979
	ASBC-I-750	7.41E-04	37.65	0.91	0.206	0.012	-883.653	0.073	5.178
Cd^{2+}	ASBC-I-550	9.30E-04	54.56	0.95	0.004	0.000	-11.707	0.002	0.008
	ASBC-I-750	6.02E-04	71.01	0.97	0.002	0.000	-26.168	0.001	0.006
		Yoon-Nelson model							
Adsorbate		K_{YN} (h^{-1})	τ (h)	R^2	SSE	RMSE	ARE	Chi-square	HYBRID
CrO_4^{2-}	ASBC-I-550	0.54	10.46	0.95	0.509	0.039	-1878.581	0.182	25.005
	ASBC-I-750	0.49	14.22	0.87	0.060	0.004	-9333.129	0.043	43.270
AsO_2^-	ASBC-I-550	0.41	9.15	0.93	0.753	0.045	-5437.260	0.285	197.924
	ASBC-I-750	0.49	10.79	0.89	0.392	0.023	-1305.203	0.155	12.136
Ni^{2+}	ASBC-I-550	0.34	12.61	0.91	0.564	0.042	-2892.621	0.225	55.979
	ASBC-I-750	0.45	12.53	0.91	0.206	0.012	-883.653	0.073	5.178
Cd^{2+}	ASBC-I-550	0.43	21.10	0.93	0.004	0.000	-11.707	0.002	0.008
	ASBC-I-750	0.36	23.90	0.97	0.002	0.000	-26.168	0.001	0.006

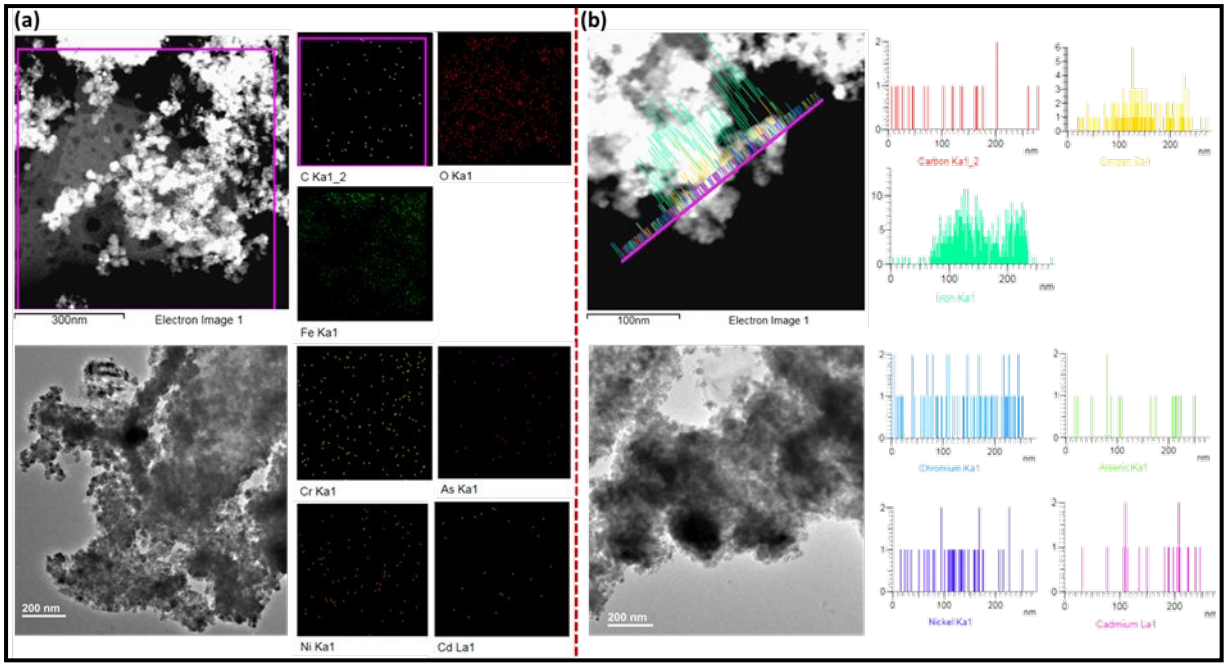

Fig. S11 (a) elemental mapping and (b) line can of ASBC-I-550 composite after the sorption of contaminants

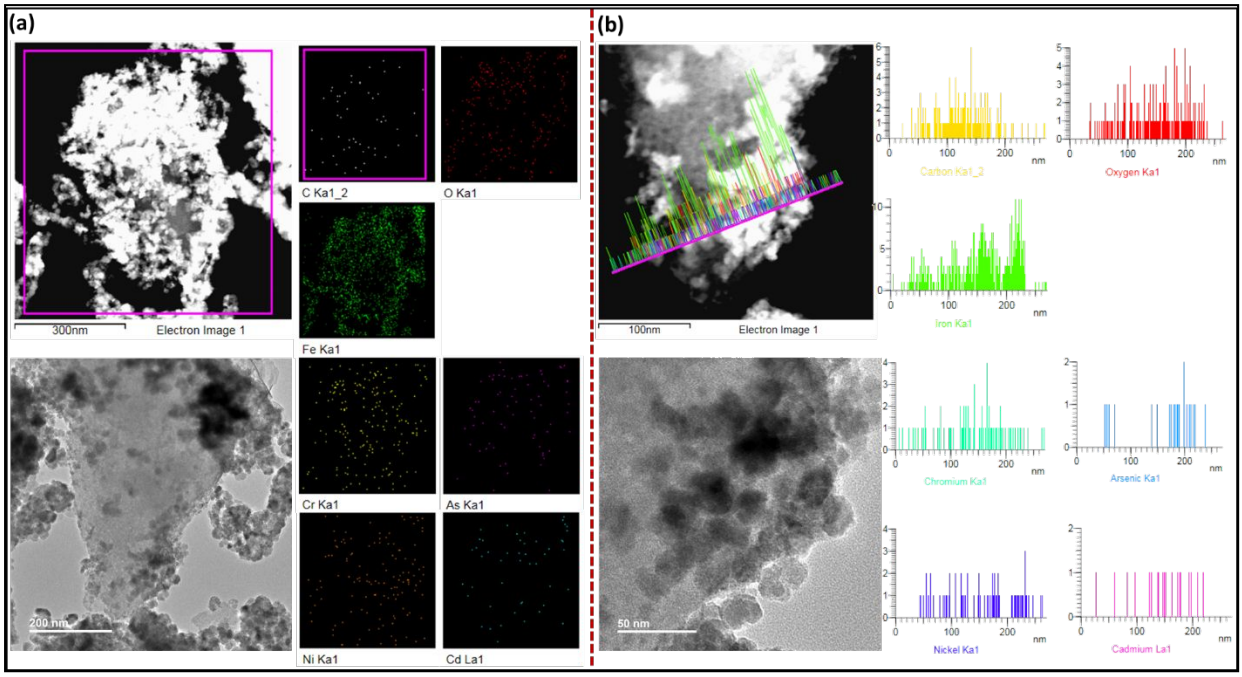

Fig. S12 (a) elemental mapping and (b) line can of ASBC-I-750 composite after the sorption of contaminants

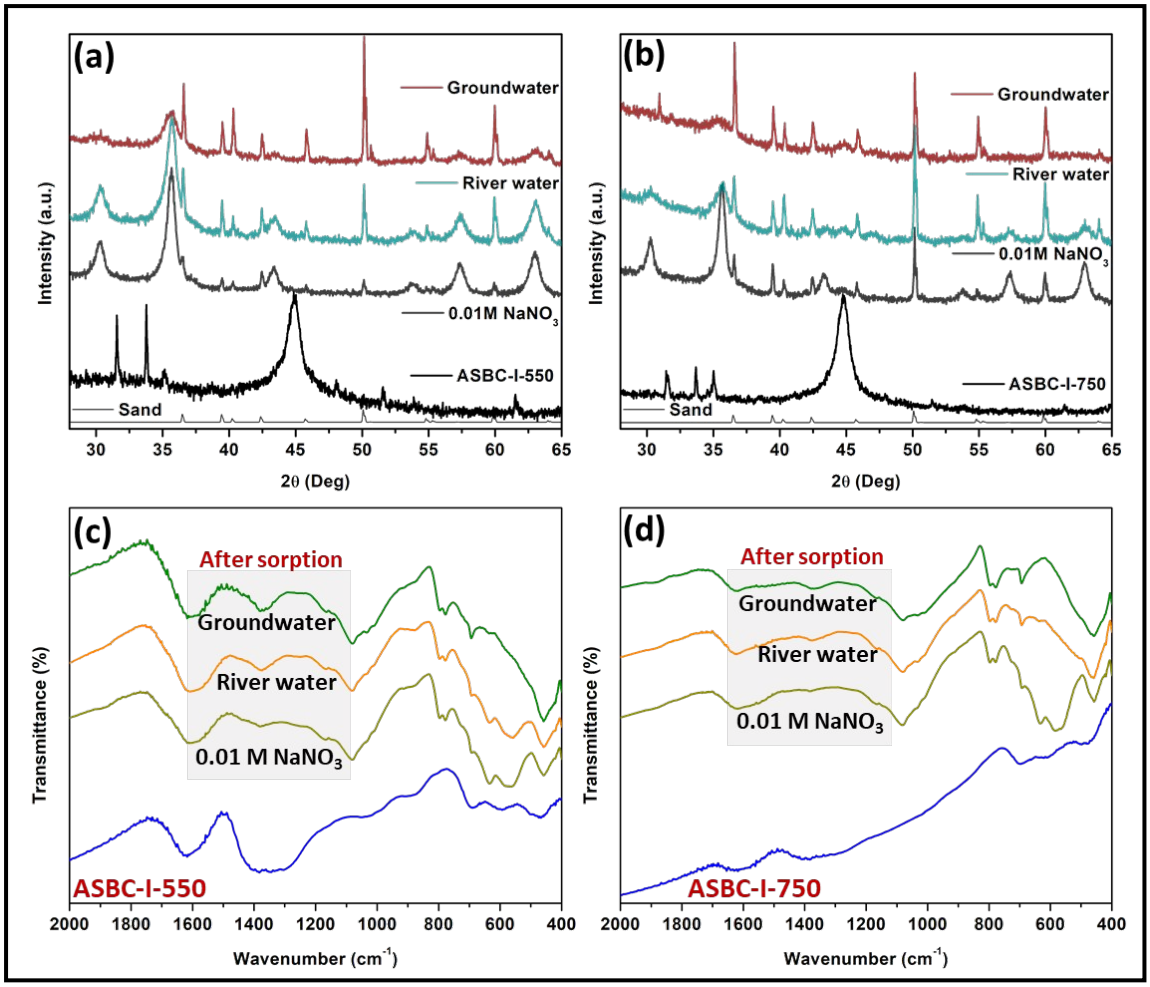

Fig. S13 (a, b) pXRD and (c, d) FTIR spectra before and after the sorption of multi-metallic species on both the composites in various aqueous matrices

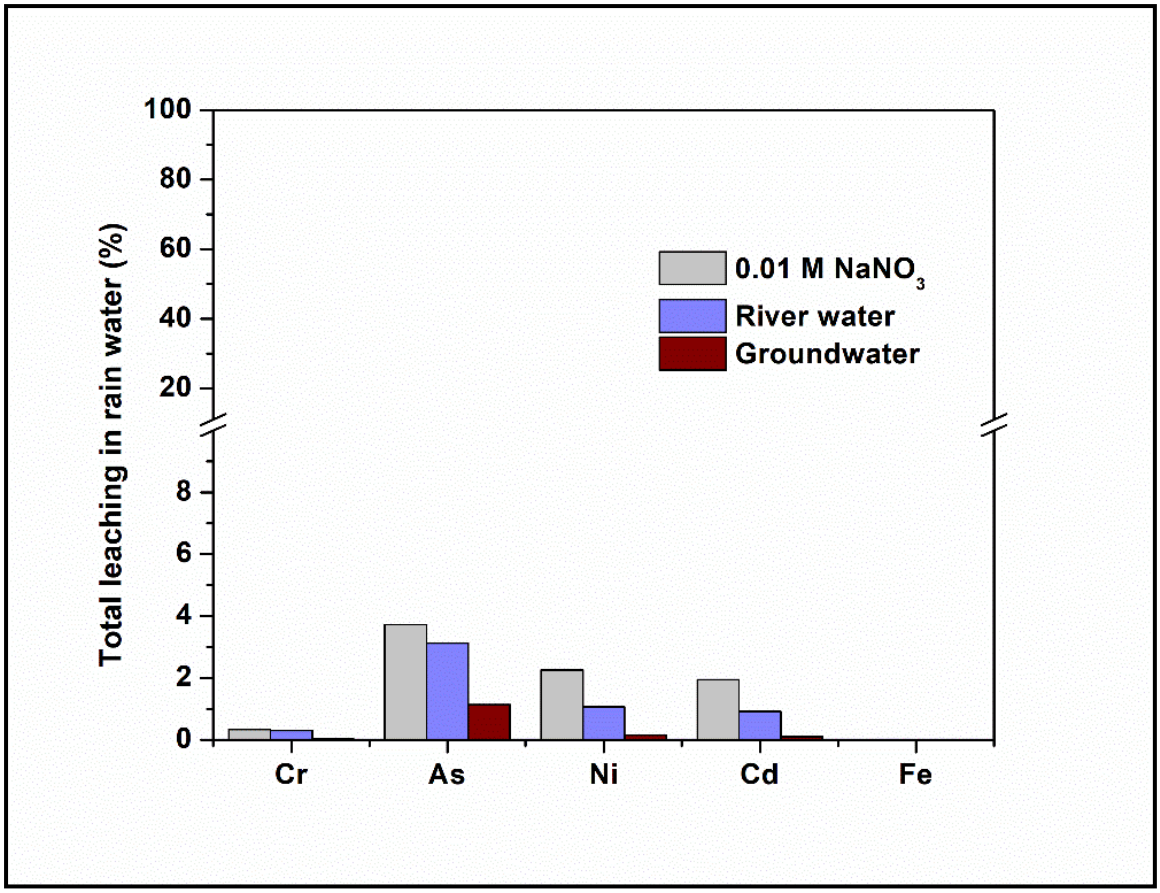

Fig. S14 Leaching of contaminants and iron in synthetic rain water solution from the spent composite

Table S12 Summary of reported adsorbents and their contaminants sorption capacities

Adsorbents	Contaminants				Reference
	Ni^{2+}	CrO_4^{2-}	AsO_2^-	Cd^{2+}	
ASBC-I-550	44.5	125.9	300.3	171.2	**This study**
ASBC-I-750	16.7	107.8	97.7	152.3	**This study**
Biochar-nZVI	47.85	23.09	-	39.53	[14]
Bentonite supported nZVI	50.25	9			[15, 16]
Bentonite-nZVI	16.5			14.25	[16]
Activated alumina		25.57			[17]
Nano- alumina	30.82	-			[18]
(nZVI)-Fe_3O_4 nanocomposites		20.41			[19]
Modified activated carbon	78.12	-			[20]
Au-nZVI				40- 188	[21]
Activated carbon (AC)		9.89			[22]
AC-nZVI		25	18.2		[22, 23]
coal fly ash-nZVI				200	[24]
Magnetic magnetite (Fe_3O_4)		20.16			[25]
Biochar-magnetite			5.49		[26]

Ascorbic acid coated Fe3O4 nanoparticles	46.06	[27]
Nanoscale Fe-Mn Binary Oxides Loaded on Zeolite	296.23	[28]

Table S13 Obtained species % from spectral fits in different elemental regions before and after sorption

Fe2p region		**Fe(II)**	**Fe(III)**	
	Before sorption	62.3	37.7	
	After sorption	58.4	41.6	
		$-OH_2$	**$-OH^-$**	**$-O_2^-$**
O1s region	**Before sorption**	3.37	87.57	9.05
	After sorption	24.7	34.4	40.9
C1s region		**-O-C=O**	**-C=O**	**C-C/ C=C**
	Before sorption	19.2	17.8	60.5
	After sorption	14.8	18.1	62.7
Cr2p		**Cr(III)**	**Cr(VI)**	
	After sorption	74.8	25.2	
As3d		**As(III)**	**As(V)**	
	After sorption	51.3	48.7	
Ni2p		**$Ni(OH)_2$**		
	After sorption	100		
Cd3d		**$Cd(OH)_2$**		
	After sorption	100		

References

1. N. Khandelwal, M. P. Behera, J. K. Rajak and G. K. Darbha, Biochar–nZVI nanocomposite: optimization of grain size and Fe 0 loading, application and removal mechanism of anionic metal species from soft water, hard water and groundwater, *Clean Technol Envir*, 2020, **22**, 1015-1024.
2. N. Khandelwal and G. K. Darbha, Combined antioxidant capping and surface support for the preservation of redox-sensitive nanoparticles: a greener way for continuous elimination of multi-metallic species, *Chem Commun*, 2021, **(In review)**.
3. N. Hemati Matin, M. Jalali, V. Antoniadis, S. M. Shaheen, J. Wang, T. Zhang, H. Wang and J. Rinklebe, Almond and walnut shell-derived biochars affect sorption-desorption, fractionation, and release of phosphorus in two different soils, *Chemosphere*, 2020, **241**, 124888.
4. A. Liu and W.-x. Zhang, Fine structural features of nanoscale zero-valent iron characterized by spherical aberration corrected scanning transmission electron microscopy (Cs-STEM), *Analyst*, 2014, **139**, 4512-4518.
5. Y. S. Ho and G. McKay, Pseudo-second order model for sorption processes, *Process Biochem*, 1999, **34**, 451-465.
6. A. G. N. Wamba, E. C. Lima, S. K. Ndi, P. S. Thue, J. G. Kayem, F. S. Rodembusch, G. S. dos Reis and W. S. de Alencar, Synthesis of grafted natural pozzolan with 3-aminopropyltriethoxysilane: preparation, characterization, and application for removal of Brilliant Green 1 and Reactive Black 5 from aqueous solutions, *Environ Sci Pollut R*, 2017, **24**, 21807-21820.
7. Y. Liu and L. Shen, A general rate law equation for biosorption, *Biochem Eng J*, 2008, **38**, 390-394.
8. J.-P. Simonin and J. Bouté, Intraparticle diffusion-adsorption model to describe liquid/solid adsorption kinetics, *Revista Mexicana De Ingenieria Quimica*, 2016, **15**, 161-173.
9. H. K. Boparai, M. Joseph and D. M. O'Carroll, Kinetics and thermodynamics of cadmium ion removal by adsorption onto nano zerovalent iron particles, *J Hazard Mater*, 2011, **186**, 458-465.
10. N. Ayawei, A. N. Ebelegi and D. Wankasi, Modelling and Interpretation of Adsorption Isotherms, *J Chem-Ny*, 2017, DOI: Artn 3039817

10.1155/2017/3039817.
11. A. Nimibofa, A. Ebelegi and W. Donbebe, Modelling and Interpretation of Adsorption Isotherms, *Hindawi Journal of Chemistry*, 2017, **Volume 2017**, 11 pages.
12. Z. Z. Chowdhury, S. M. Zain, A. K. Rashid, R. F. Rafique and K. Khalid, Breakthrough Curve Analysis for Column Dynamics Sorption of Mn(II) Ions from Wastewater by Using Mangostana garcinia Peel-Based Granular-Activated Carbon, *J Chem-Ny*, 2013, **2013**, 959761.
13. S. Chang, H. Fu, X. Wu, C. Liu, Z. Li, Y. Dai and H. Zhang, Batch and fixed-bed column studies for selective removal of cesium ions by compressible Prussian blue/polyurethane sponge, *RSC Advances*, 2018, **8**, 36459-36467.
14. S. S. Zhu, S. H. Ho, X. C. Huang, D. W. Wang, F. Yang, L. Wang, C. Y. Wang, X. D. Cao and F. Ma, Magnetic Nanoscale Zerovalent Iron Assisted Biochar: Interfacial Chemical Behaviors and Heavy Metals Remediation Performance, *Acs Sustain Chem Eng*, 2017, **5**, 9673-9682.
15. L. N. Shi, X. Zhang and Z. L. Chen, Removal of Chromium (VI) from wastewater using bentonite-supported nanoscale zero-valent iron, *Water Res*, 2011, **45**, 886-892.
16. N. A. Zarime, W. Z. W. Yaacob and H. Jamil, Removal of heavy metals using bentonite supported nano-zero valent iron particles, *AIP Conference Proceedings*, 2018, **1940**, 020029.

17. A. K. Bhattacharya, T. K. Naiya, S. N. Mandal and S. K. Das, Adsorption, kinetics and equilibrium studies on removal of Cr(VI) from aqueous solutions using different low-cost adsorbents, *Chem Eng J*, 2008, **137**, 529-541.
18. V. Srivastava, C. H. Weng, V. K. Singh and Y. C. Sharma, Adsorption of Nickel Ions from Aqueous Solutions by Nano Alumina: Kinetic, Mass Transfer, and Equilibrium Studies, *Journal of Chemical & Engineering Data*, 2011, **56**, 1414-1422.
19. X. S. Lv, Y. J. Hu, J. Tang, T. T. Sheng, G. M. Jiang and X. H. Xu, Effects of co-existing ions and natural organic matter on removal of chromium (VI) from aqueous solution by nanoscale zero valent iron (nZVI)-Fe3O4 nanocomposites, *Chem Eng J*, 2013, **218**, 55-64.
20. M. O. Abd El-Magied, A. M. A. Hassan, H. M. H. Gad, T. F. Mohammaden and M. A. M. Youssef, Removal of nickel (II) ions from aqueous solutions using modified activated carbon: A kinetic and equilibrium study, *Journal of Dispersion Science and Technology*, 2018, **39**, 862-873.
21. Y. Su, A. S. Adeleye, Y. Huang, X. Sun, C. Dai, X. Zhou, Y. Zhang and A. A. Keller, Simultaneous removal of cadmium and nitrate in aqueous media by nanoscale zerovalent iron (nZVI) and Au doped nZVI particles, *Water Res*, 2014, **63**, 102-111.
22. S. Mortazavian, H. An, D. Chun and J. Moon, Activated carbon impregnated by zero-valent iron nanoparticles (AC/nZVI) optimized for simultaneous adsorption and reduction of aqueous hexavalent chromium: Material characterizations and kinetic studies, *Chem Eng J*, 2018, **353**, 781-795.
23. H. Zhu, Y. Jia, X. Wu and H. Wang, Removal of arsenic from water by supported nano zero-valent iron on activated carbon, *J Hazard Mater*, 2009, **172**, 1591-1596.
24. L. Ma, Q. Wei, Y. Chen, Q. Song, C. Sun, Z. Wang and G. Wu, Removal of cadmium from aqueous solutions using industrial coal fly ash-nZVI, *Roy Soc Open Sci*, 2018, **5**, 171051-171051.
25. S. Rajput, C. U. Pittman, Jr. and D. Mohan, Magnetic magnetite (Fe3O4) nanoparticle synthesis and applications for lead (Pb2+) and chromium (Cr6+) removal from water, *J Colloid Interface Sci*, 2016, **468**, 334-346.
26. C. M. Navarathna, A. G. Karunanayake, S. R. Gunatilake, C. U. Pittman, F. Perez, D. Mohan and T. Mlsna, Removal of Arsenic(III) from water using magnetite precipitated onto Douglas fir biochar, *J Environ Manage*, 2019, **250**, 109429.
27. L. Feng, M. Cao, X. Ma, Y. Zhu and C. Hu, Superparamagnetic high-surface-area Fe3O4 nanoparticles as adsorbents for arsenic removal, *J Hazard Mater*, 2012, **217-218**, 439-446.
28. S. Kong, Y. Wang, Q. Hu and A. K. Olusegun, Magnetic nanoscale Fe–Mn binary oxides loaded zeolite for arsenic removal from synthetic groundwater, *Colloids and Surfaces A: Physicochemical and Engineering Aspects*, 2014, **457**, 220-227.